




Microscopic adaptation of BaHfO₃ and Y₂O₃ artificial pinning centers for strong and isotropic pinning landscape in YBa₂Cu₃O_{7-x} thin films

Bibek Gautam^{1,5} , Mary Ann Sebastian², Shihong Chen^{1,3} , Timothy Haugan², Wenrui Zhang⁴, Jijie Huang⁴ , Haiyan Wang⁴ and Judy Z Wu^{1,5}

¹ Department of Physics and Astronomy, University of Kansas, Lawrence, KS 66045, United States of America

² U.S. Air Force Research Laboratory, Aerospace Systems Directorate, WPAFB, OH 45433 United States of America

³ College of Engineering and Applied Science, Nanjing University, Nanjing, Jiangsu 210093, People's Republic of China

⁴ School of Materials Engineering, Purdue University, West Lafayette, IN 47907, United States of America

E-mail: gautibe@ku.edu and jwu@ku.edu

Received 25 September 2017, revised 14 November 2017

Accepted for publication 12 December 2017

Published 11 January 2018



CrossMark

Abstract

A study of 3 vol% Y₂O₃ + 2–6 vol% BaHfO₃ double-doped YBa₂Cu₃O_{7-x} (BHO DD) epitaxial thin films was carried out to explore the morphology adaption of *c*-axis aligned one-dimensional BHO artificial pinning centers (1D APCs) to secondary Y₂O₃ nanoparticles (3D APCs). BHO 1D APCs have been predicted to have the least rigidity in an elastic strain energy model in APC/YBa₂Cu₃O_{7-x} nanocomposite films. Consequently, they could be best ‘tuned’ away from the *c*-axis alignment by local strains generated by the Y₂O₃ 3D APCs. This provides an opportunity to generate mixed-morphology APCs, especially at high BHO concentrations. Motivated by this, we have carried out a systematic study of the transport critical current density $J_c(H, T, \theta)$ on the BHO DD samples in magnetic fields (H) up to 90 kOe at different H orientations from $H//c$ -axis ($\theta = 0^\circ$), to $\theta = 45^\circ$, and to $H//ab$ -plane ($\theta = 90^\circ$). Enhanced pinning at all three orientations was observed as illustrated in the comparable low α (α) values in the range of 0.13–0.25 at 65 K, which is consistent with the mixed 1D (in *c*-axis) + 2D (in *ab*-plane) + 3D APCs observed in transmission electron microscopy (TEM). Upon increasing BHO concentration from 2 to 4 vol%, a monotonic increase of the accommodation field H^* at $\theta = 0^\circ$, 45° and 90° was observed, indicative of the APC concentration increase of the mixed morphologies. At 6 vol% BHO, the H^* continues the increase to 85 kOe at $H//c$ -axis ($\theta = 0^\circ$), and >90 kOe $H//ab$ -plane ($\theta = 90^\circ$), while it decreases from 80 to 85 kOe at 2–4 vol% to 60 kOe at 6 vol% at $\theta = 45^\circ$, which is consistent with the TEM observation of the connection of 3D APCs, appeared at lower BHO concentration into 2D ones in *ab*-plane at the higher BHO concentrations. These results shed light on the quantitative adaptation of APCs of mixed morphologies with increasing BHO doping in the BHO DD thin films and are important for controlling the APC pinning landscape towards minimal angular dependence.

Keywords: YBCO, isotropic pinning, J_c anisotropy, mixed-morphology APCs

(Some figures may appear in colour only in the online journal)

⁵ Authors to whom any correspondence should be addressed.

Introduction

As we know, *c*-axis aligned one-dimensional artificial pinning centers (1D APCs) such as BaZrO₃ (BZO) [1–5], BaSnO₃ (BSO) [1, 6, 7], YBa₂(Nb/Ta)O₆ [8, 9], and BaHfO₃ (BHO) in high temperature superconducting (HTS) (Y/Gd/Sm)BaCu₃O_{7-x} [1, 10–14] films and coated conductors [15–18], provide strong correlated pinning, typically illustrated as a peak of the critical current density J_c at $H//c$ -axis. However, the pinning efficiency of these 1D APCs reduces dramatically when H orientation is away from the *c*-axis. In order to reduce the angular dependence of the J_c , generation of APCs with mixed morphologies has been explored recently [17, 19–24]. Among others, double doping (DD) of 1D + 3D APCs (nanoparticles), such as BSO + Y₂O₃ [17, 22, 24] and BZO + Y₂O₃ [19, 20] in (Y/Gd/Sm)BaCu₃O_{7-x}, has been identified as an effective approach to reduce the angular dependence of J_c stemming originally from the layered structure of the HTS materials. In these DD samples, the BZO and BSO 1D APCs are anticipated to primarily maintain their 1D morphology and orientation in *c*-axis since they are highly rigid. Nevertheless, shorter and misaligned BZO 1D APCs were reported in the BZO DD samples as compared to the single-doping (SD) case without Y₂O₃ in YBaCu₃O_{7-x} (YBCO) [25, 26]. The mixed (1D + 2D + 3D) APCs morphology is important to enhance the minimum J_c ($J_{c,min}$) value by providing strong pinning in the entire angular range from $\theta = 0^\circ$ ($H//c$ -axis) to 90° ($H//ab$ -plane) for the magnetic field orientations (θ is defined as the angle between H and the *c*-axis in the plane perpendicular to J_c). Enhanced pinning indeed has been observed in the DD samples. In the BSO DD samples, Jha *et al* reported the enhanced $J_c(H//c) \sim 1.7 \text{ MA cm}^{-2}$ at 65 K and 40 kOe from the concentration of BSO DD samples with 3.0 vol% BSO + 3.0 area% Y₂O₃ in YBCO as compared to the BSO SD YBCO counterparts [27]. Horide *et al* reported the similar enhancement of $J_c(H//c)$ at same field 40 kOe for 4 wt% BSO and 2.4 area% Y₂O₃ doped YBCO compared to 4 wt% BSO doped YBCO [17]. This high $J_c(H//c)$ was due to the high rigidity of BSO to form *c*-axis aligned 1D APCs even in the presence of Y₂O₃ 3D APCs. In fact, Jha *et al* reported that the J_c -anisotropy was reduced to 82% for the same DD YBCO sample from 181% for 3 vol% BSO SD YBCO sample at 77 K, and 10 kOe [27].

In these 1D + 3D APC DD samples, doping high-concentration 1D APCs may encounter the same issue of strain field overlap of perfectly *c*-axis aligned 1D APCs as in the SD case. This can lead to considerable degradation of the critical temperature T_c and prevent applications at high temperatures near 77 K [28–30]. The strain field overlap may be reduced by splaying 1D APCs or even switching their orientation away from the *c*-axis to *ab*-plane via application of a tensile strain in the *ab*-plane of the YBCO matrix on vicinal substrates. This yields a mixed 1D (in *c*-axis with a splay angle) + 2D (in *ab*-plane) APCs with smaller T_c degradation and a higher overall J_c at 77 K across the entire H orientation range as compared to the nonvicinal counterparts' [21, 23, 31]. On the other hand, a similar tuning on the 1D APCs may be achieved

more readily if the 1D APCs with lower rigidity are selected in the DD samples. Among others, BHO 1D APCs have the least rigidity based on the simulation using an elastic strain model [32–34]. In a recent exploratory study [34], transport J_c was investigated in YBCO films doped with BHO (2.0 vol%) + Y₂O₃ (3.0 vol%) (BHO DD) or BZO (2.0 vol%) + Y₂O₃ (3.0 vol%) (BZO DD) respectively. The much more reduced J_c anisotropy in the former is ascribed to the mixed 1D (in *c*-axis with a splay angle) + 2D (in *ab*-plane) + 3D APC morphologies due to the higher tunability or lesser rigidity of BHO 1D APCs compared to its BZO counterparts. Motivated by this result, this work investigates BHO DD thin films at a variable BHO concentration in the range of 2.0–6.0 vol% and a fixed concentration of Y₂O₃ (3.0 vol%). With an increasing BHO concentration in the DD samples, we aim to understand the effect of the APC concentration on the mixed 1D + 2D + 3D APCs morphology. By measuring the $J_c(H)$ at $\theta = 0^\circ$ ($H//c$ -axis), 45° and $\theta = 90^\circ$ ($H//ab$ -plane), and correlating the $J_c(H)$ results with the microstructures of these samples observed using transmission electron microscopy (TEM), we have observed an increasing switch of the BHO 1D APCs from *c*-axis aligned to *ab*-aligned with increasing BHO concentration. The overall best $J_c(H, \theta)$ was observed on the 4 vol% BHO DD film in the field range of 0–90 kOe and at 65–77 K, which is attributed to the mixed 1D + 2D + 3D APC morphologies of quantitatively optimal APC concentrations.

Sample preparation and experiment

BHO DD thin films with fixed 3.0 vol% Y₂O₃ doping mixed with 2.0, 4.0, and 6.0 vol% of BHO doping in YBCO were fabricated at an optimal substrate temperature of 810 °C with oxygen partial pressure of 300 mTorr using pulsed laser deposition (PLD) on (100) SrTiO₃ (STO) single crystal substrates. The film thicknesses of 120–140 nm were confirmed using Tencor profilometer. The details of the sample fabrication procedure have been reported previously [19, 34]. For convenience, the samples with three different BHO concentrations will be regarded as 2% BHO DD, 4% BHO DD and 6% BHO DD in the rest of the paper. It should be realized while the volume proportion of the BHO APCs is proportional to the BHO content in the BHO + YBCO target, its specific value detectable using electron microscopy is sensitively affected by the PLD growth conditions such as temperature, growth rate and other parameters [31]. For the transport J_c measurements, two parallel microbridges of widths $\sim 20 \mu\text{m}$ and $\sim 40 \mu\text{m}$, respectively, and length $\sim 500 \mu\text{m}$ were patterned using standard photolithography. Current–voltage (I – V) characteristics of these films were measured using Keithley 2430 1 KW pulsed current source meter and HP 34420 a nanovoltmeter. The short pulse of 50 ms at the interval of 3.0–4.0 s was utilized to minimize the heating effect in the samples. The critical transition temperatures (T_c) were measured with a Quantum Design Evercool II Physical Properties Measurement System (PPMS) with a vibrating sample magnetometer probe. The J_c as a function of temperature T , magnetic field H , and H orientation θ was

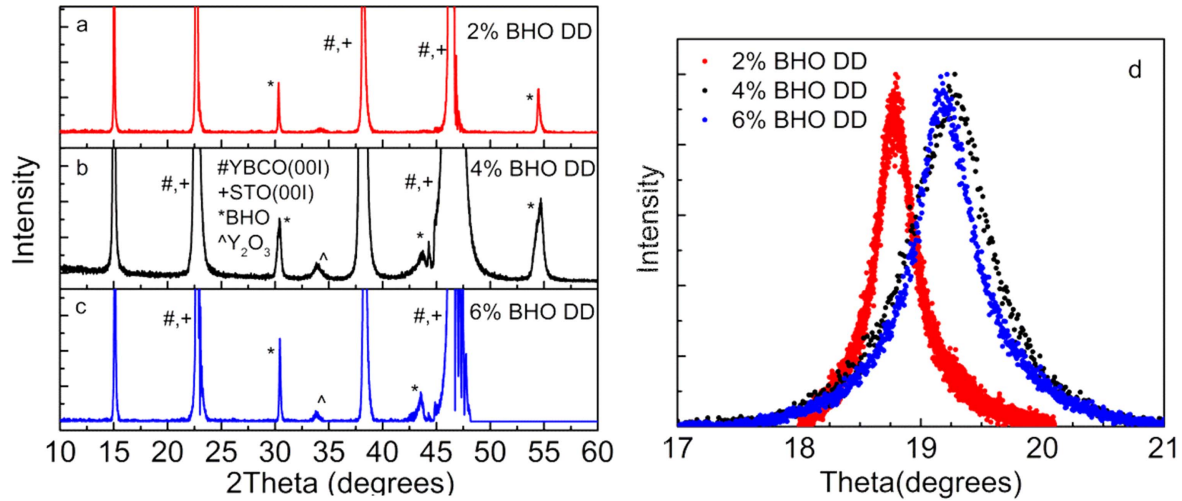


Figure 1. (a)–(c) XRD θ – 2θ spectra for the 2% BHO DD (red), 4% BHO DD (black), and 6% BHO DD (blue) nanocomposite films on STO substrates and (d) rocking curve of YBCO (005) peak of the same nanocomposite films. Color codes follow the same for both figures.

Table 1. Critical temperature (T_c), c -axis lattice constant, FWHM of the YBCO (005) rocking curve, and J_c anisotropy of 2%, 4%, and 6% BHO DD films.

Samples	$T_{c,onset}$ (K)	c -axis lattice constant (nm)	FWHM of the YBCO (005) rocking curve	J_c anisotropy		
				77 K	65 K	
					50 kOe	90 kOe
2% BHO DD	87.08	1.177	0.353	0.41	0.47	0.18
4% BHO DD	86.60	1.175	0.759	1.04	0.42	0.56
6% BHO DD	85.80	1.173	0.567	4.21	1.11	1.73

calculated using the standard $1 \mu\text{V cm}^{-1}$ criterion in the PPMS. In particular, $J_c(H)$ curves were taken at $\theta = 0^\circ$ ($H//c$ -axis), 45° , and 90° ($H//ab$ -plane) at different magnetic fields up to 90 kOe in the temperature range of 65–77 K in order to quantify the pinning anisotropy as function of the BHO doping. TEM images were obtained using a FEI Tecnai F20 analytical microscope using acceleration voltage of 200 kV while x-ray diffraction (XRD) spectra were taken and analyzed using Bruker D8 Discover diffractometer.

Result and discussion

Figures 1(a)–(c) compare the XRD θ – 2θ spectra for the 2% BHO DD (red), 4% BHO DD (black), and 6% BHO DD (blue) samples respectively. All samples show high quality crystallinity with c -axis orientation as illustrated in the appearance of the YBCO (001) peaks. The minor peaks at around $2\theta \sim 30^\circ$ and $\sim 43^\circ$ could be indexed to the BHO and the minor peak at around $2\theta \sim 34^\circ$ could be indexed to the Y_2O_3 phases. The c -axis lattice constants of YBCO films were calculated from figures 1(a)–(c) and the results are listed in table 1. Highly coherent APC/YBCO interface is maintained at low BHO doping of 2 vol% in these samples as expected, which is confirmed by an elongated c -axis of 11.77 Å. With a further increased doping of BHO, the c -axis

lattice is reduced systematically towards 11.68 Å for an undoped YBCO. BHO SD YBCO thin film [35], in which c -axis lattice constant increases from ~ 11.69 to ~ 11.72 Å when BHO concentration increases from 2 to 6 mol% (corresponding to ~ 1 to 3 vol%), in contrast to BHO DD films. Figure 1(d) depicts the XRD (005) rocking curves of these samples with the same color codes as in figures 1(a)–(c). A shift of the (005) peak towards right (larger θ) is an indication of the decrease of the c -axis lattice constant with BHO concentration. Consistently, an initial increase of the YBCO (005) full width at half maximum (FWHM) with increasing BHO concentration in the lower BHO doping range of 2–4 vol% (0.353 at 2% and 0.759 at 4%) is an indication of an increasing lattice strain while a coherent or semi-coherent BHO/YBCO interface is maintained in this doping range. At the higher BHO doping of 6 vol%, a reduced (005) FWHM of 0.567 was observed. This reversed trend suggests the released lattice strain due to formation of defects at the BHO/YBCO interface, which is consistent with the reduced c -axis elongation in 6% DD sample as compared to that of the 4% DD sample (table 1). The formation of defects such as dislocations, especially at the APC/YBCO interfaces, leads to relaxation of the interfacial strain, resulting in less elongated c -axis and increased FWHM of the (005) YBCO peak [36–39]. In addition, the T_c decreases monotonically (table 1) with the BHO doping from ~ 90 K for the undoped YBCO

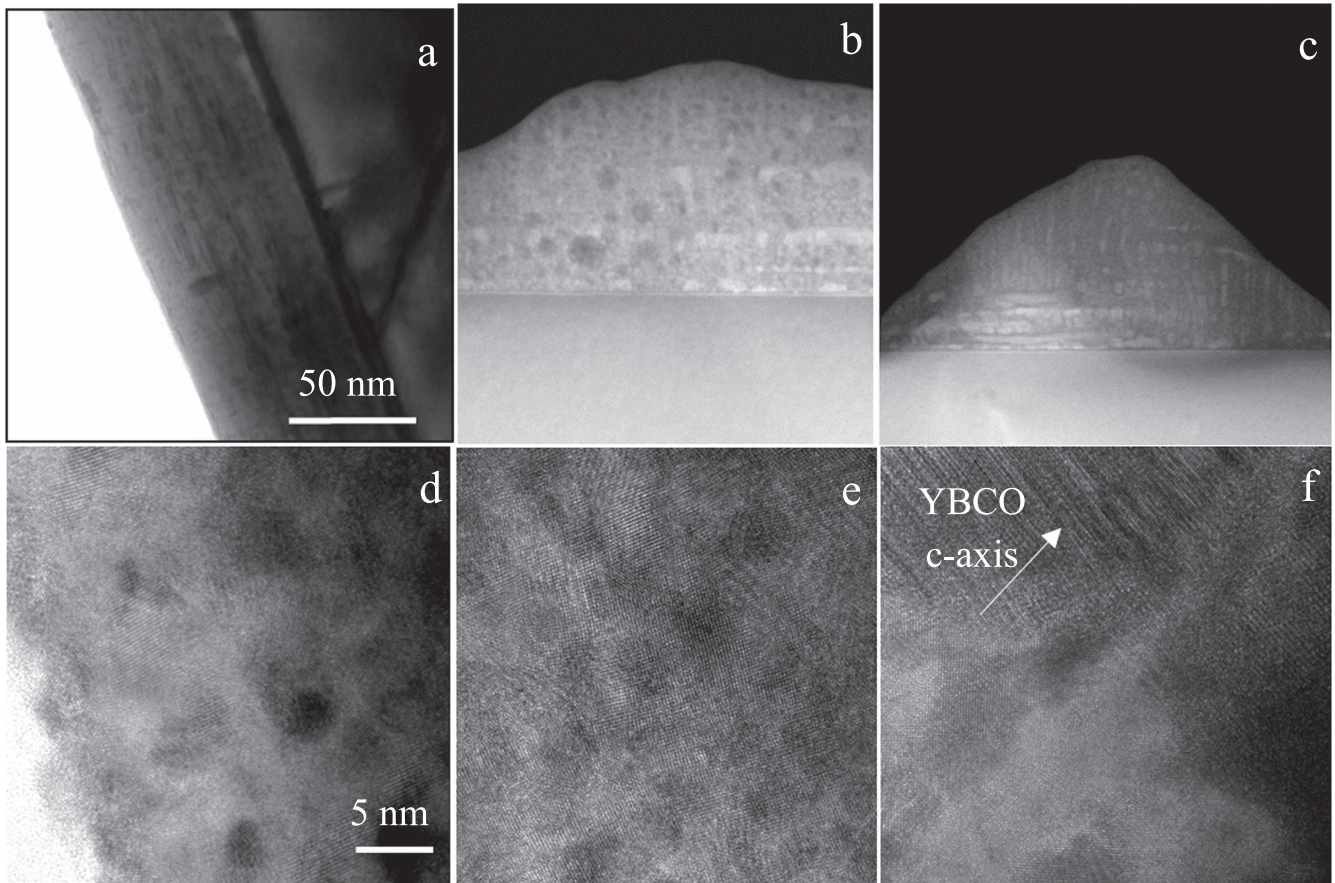


Figure 2. TEM images of 2%, 4% and 6% BHO DD nanocomposite films (a), (b) and (c) at low magnification respectively, (d), (e) and (f) at high magnification respectively. Scale bar 50 nm is same for figures (a)–(c) and 5 nm is same for figures (d)–(f).

films to 87.1 K, 86.6 K, and 85.8 K for 2%, 4%, and 6% BHO DD samples respectively. In comparison with the BHO SD samples [35, 40] in which the T_c values also decrease monotonically with the BHO doping, from 88.1 to 87.7 K when BHO concentration increases from 2 to 6 mol% (corresponding to ~ 1 to 3 vol%), a comparable but slightly higher T_c degradation occurs in the BHO DD samples.

Figures 2(a)–(f) show the low and high magnification cross-sectional TEM images of the 2% (a), (d), 4% (b), (e) and 6% (c), (f) BHO DD films, respectively. In figure 2(a), high-concentration BHO 1D APCs (c -axis aligned), and moderate-concentration BHO 2D APCs (ab -aligned) are observed. Aside from these BHO 1D + 2D APCs, 3D APCs (spherical and irregular shaped nanostructures) of several nanometers in dimension are primarily attributed to be Y_2O_3 and possibly BHO nanoparticles (figure 2(d)). This confirms the mixed APCs landscape in 2% BHO DD films, which is in contrast to the typically only c -axis aligned BHO 1D APCs in the BHO SD films [1]. In addition, while a mixed 1D + 3D APCs morphology was reported in 2 vol% BZO DD film by Maiorov *et al* [25], the appearance of the ab -aligned 2D APCs in BHO DD case suggests the higher tunability of the BHO APCs by the secondary Y_2O_3 dopant. This argument is consistent with the higher 2D BHO APCs observed BHO DD samples with higher BHO concentrations.

As the BHO concentration is increased to 4 vol% in the BHO DD samples, the APC morphology becomes more

mixed with a large number of 1D, 2D and 3D APCs visible clearly in figure 2(b). Many through-thickness 1D APCs are truncated by 2D APCs in the ab -plane into shorter segments along the c -axis. Some of these 1D and 2D APCs are not connected, with 3D APCs located in between the nearest neighbors. A zoom-in view of the microstructure of the 4% BHO DD sample in figure 2(e) reveals the APCs typically have their smaller dimension on the order of 5–10 nm. Since the Y_2O_3 doping is the same in all BHO DD samples, the increased 2D and 3D APC concentrations in the 4% BHO DD sample as compared to the 2% BHO DD sample indicates the increased BHO doping increases the concentrations of 1D, 2D and 3D APCs proportionally. This trend of switching of 1D BHO APCs to other morphologies continues with increasing BHO concentrations. At 6 vol% BHO higher concentration and more continuous 2D APCs in the ab -plane are clearly seen (figures 2(c) and (f)), in addition to shorter BHO 1D APCs along c -axis together with 3D APCs. Based on the TEM observation, it can be concluded that in BHO DD films, mixed morphologies of 1D, 2D, and 3D APCs are formed as illustrated schematically in figure 3.

Figures 4(a)–(c) compare the $J_c(H)$ curves measured on 2%, 4% and 6% BHO DD films at B orientations $\theta = 0^\circ$ ($H//c$ -axis), $\theta = 45^\circ$ and $\theta = 90^\circ$ ($H//ab$ -plane) at 77 K (solid) and figures 4(d)–(f) compare $J_c(H)$ for the same samples at the same field orientation and at 65 K (open). At $\theta = 0^\circ$, the 4% BHO DD film (black) has the highest $J_c(H)$ at both 77 and

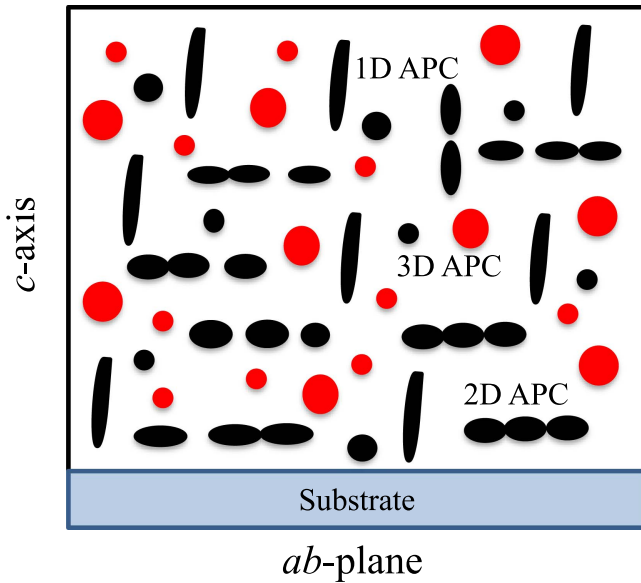


Figure 3. Schematic of the microstructure distribution in the c -oriented BHO double-doped YBCO film matrix. Color codes: BHO 1D, 2D and 3D APCs (black), Y_2O_3 3D APCs (red).

65 K despite having a slightly lower T_c than that of the 2% BHO DD sample. Interestingly, the $J_c(H)$ curves for the 2% and 4% BHO DD films have qualitatively similar trends at 77 K and 65 K respectively. The different qualitative trend of the $J_c(H)$ curve for the 6% BHO DD sample at 77 K may be attributed partly to the lower T_c of this sample (the lowest among the three as shown in table 1) since the three samples have a similar trend in $J_c(H)$ curves at the lower temperature of 65 K. However, the lower $J_c(H)$ values of the 6% BHO DD sample at 65 K may be partly due to the reduced concentration of the c -axis aligned BHO 1D APCs and reduced pinning efficiency of very short BHO 1D APC segments.

When fitting the $J_c(H)$ curves by $J_c(H) \sim H^{-\alpha}$, lower α -values are observed on 2%–4% BHO DD samples as compared to the typical $\alpha \sim 0.5$ for undoped YBCO reference samples [4, 41, 42]. At 77 K, the α -values (table 2) for the 2% and 4% BHO DD films are 0.26 and 0.35 respectively, indicative of an enhanced correlated pinning by the c -axis aligned BHO 1D APCs. These values decrease further to 0.16 and 0.13 respectively at 65 K for these two samples, suggesting a further enhanced pinning efficiency of the BHO 1D-APCs and Y_2O_3 3D APCs at lower temperatures. In contrast, a significantly higher $\alpha \sim 0.64$ value was observed on the 6% BHO DD film at 77 K, while it is slightly higher but comparable ($\alpha \sim 0.2$) to that of 2% (0.16) and 4% (0.13) BHO DD films at 65 K. This supports our earlier argument of the combined effect of the lower T_c and lower pinning efficiency of the short c -axis aligned BHO 1D APCs in this sample. It means a portion of c -axis aligned BHO 1D APCs switches to the ab -plane aligned at the high BHO concentration of 6% which reflects on the high J_c observed in this film at the $H//ab$ -plane (figures 4(c) and (f)).

The mixed APC morphologies shown in the TEM analysis (figure 2) of the BHO DD samples are expected to

change the anisotropy of J_c considerably. In contrast to the BHO SD samples in which BHO APCs are long 1D APCs aligned along the c -axis only, the BHO APCs in the DD samples have mixed morphologies of 1D short segments of BHO along the c -axis for strong correlated pinning in c -axis and irregular shaped APCs of BHO and Y_2O_3 that can provide pinning along other directions. Quantitatively, the concentration of the c -axis aligned 1D BHO APCs increases with BHO doping in the range of 2–6 vol% (see more detailed discussion in figure 5 on discussion of H_{\max} at $\theta = 0^\circ$). The similar increase of the concentration of the irregular shaped 3D APCs explains the strong pinning at $\theta = 45^\circ$ in 2% and 4% BHO DD samples, while leads to their merge into planar APCs along the ab -plane in the 6% BHO DD sample. This results in decrease (increase) of the 3D (2D) APCs as the BHO doping is increased from 4 to 6 vol%.

Figures 4(g)–(i) compare the pinning force density $F_p (=J_c \times H)$ calculated from the $J_c(H)$ curves in figures 3(a)–(f) for the given temperatures and field orientation. At $H//c$ -axis (figure 4(g)), the highest $J_c(H)$ of the 4% BHO DD film at both 77 and 65 K lead to the highest overall $F_p(H)$ values as well. All $F_p(H)$ curves shown in figures 4(g)–(i) have an inverted bell shape with the peak value defined as $F_{p,\max}$ at H_{\max} that is comparable to the H^* . The accommodation field H^* was estimated from the F_p peak field in the F_p – H curve. At $H//c$ -axis and 65 K (T_c effect is minimal), the $F_{p,\max} \sim 68.0 \text{ GN m}^{-3}$ at $H_{\max} \sim 75 \text{ kOe}$ can be observed for the 4% BHO DD film, which is higher than the 60.4 GN m^{-3} and 45 kOe of the BHO SD films with the comparable doping [1], illustrating the benefit of the DD in terms of both enhanced APC concentration as well as overall pinning efficiency. In addition, increasing BHO concentration beyond $\sim 4\%$ adds on additional APCs as reflected in the further enhanced $H_{\max} \sim 85 \text{ kOe}$ for 6% BHO DD at 65 K. This monotonic increase of the H_{\max} with BHO doping at 65 K (to minimize the T_c effect) and $H//c$ -axis is depicted in figure 5(a). While the additional BHO doping adds additional APCs efficient of pinning at $\theta = 0^\circ$ and 65 K, the pinning efficiency decreases as shown in figure 5(b) from the best $F_{p,\max}$ of $\sim 68.0 \text{ GN m}^{-3}$ in the 4% BHO DD film to $\sim 46.0 \text{ GN m}^{-3}$ for the 6% BHO DD film, indicating the additional 2 vol% BHO doping in the latter may not form through thickness BHO 1D APCs as expected and confirmed in TEM.

At $\theta = 45^\circ$ (figures 4(b) and (e)), the $J_c(H)$ curves for the 2%, 4%, and 6% BHO DD samples have similar trends at 77 and 65 K to the case of $\theta = 0^\circ$, except less H susceptibility of $J_c(H)$ for the 6% BHO DD film. In addition, the three $J_c(H)$ curves almost overlap at the lower temperature of 65 K, indicative of similar pinning mechanism at these BHO concentrations. This argument is consistent to the comparable α values of 0.25, 0.23, and 0.24 (table 1) for the 2%, 4%, and 6% BHO DD films respectively at 65 K. However, the $F_p(H)$ at $\theta = 45^\circ$ (figure 4(h)) reveals different H_{\max} values for these three samples although the difference in their $F_{p,\max}$ values is considerably smaller than in the $\theta = 0^\circ$ case. As shown in figure 5(b), the 4 vol% BHO DD sample has the highest $F_{p,\max}$ of 45.0 GN m^{-3} , which is considerably lower than that

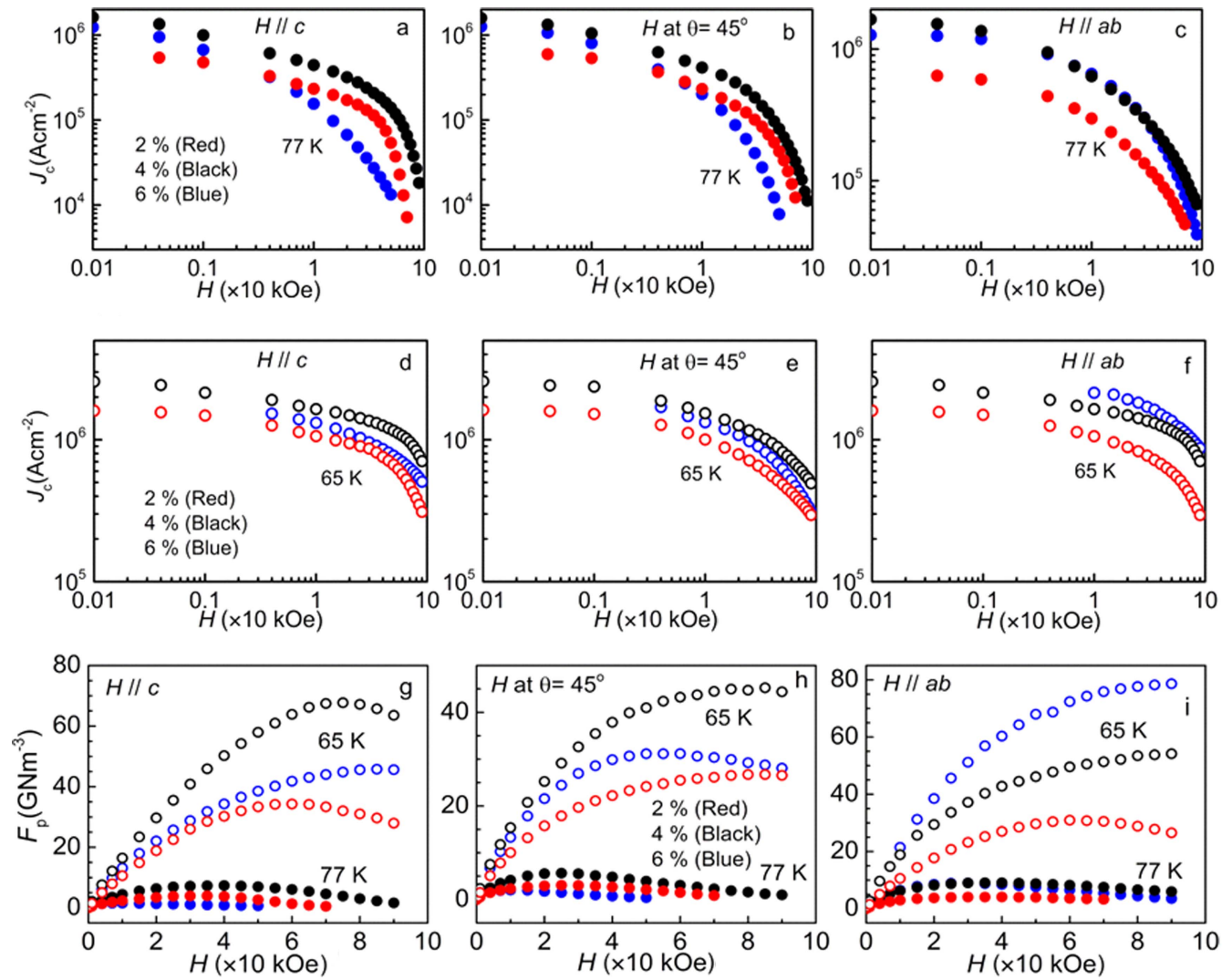


Figure 4. J_c versus H and F_p versus H curves measured on 2%, 4% and 6% BHO DD nanocomposite films at (a), (d) and (g) $\theta = 0^\circ$ ($H//c$ -axis); (b), (e) and (h) $\theta = 45^\circ$, and (c), (f) and (i) $\theta = 90^\circ$ ($H//ab$ -plane) at 77 K (solid) and 65 K (open), respectively. Color codes follow the same for all figures.

at $\theta = 0^\circ$. This is anticipated since the correlated pinning provided by the c -axis aligned BHO 1D APCs is typically stronger than that by 3D APCs at $\theta = 45^\circ$. The 2% and 6% BHO DD samples have a comparable $F_{p,max}$ of $\sim 28 \text{ GN m}^{-3}$ and 31 GN m^{-3} respectively, which is about 50% of that for the 4% BHO DD sample. Moreover, the comparable $H_{max} \sim 80$ and 85 kOe at 65 K for 2% and 4% respectively show similar or comparable concentration of 3D APCs effective for vortex pinning (figure 5(a)). However, the drop to the lowest $H_{max} \sim 60 \text{ kOe}$ for the 6% BHO DD film indicates the reduced concentration of 3D APCs, which could be Y_2O_3 nanoparticles and short/misaligned segment of 1D BHO APCs. Assuming the Y_2O_3 3D APCs concentration is not changed in the three DD samples, the decrease in the concentration of 3D APCs may be attributed to the complete switch of c -axis aligned BHO 1D APCs to ab -aligned 2D APCs in the 6% BHO via connection of those segmented ab -aligned APCs in 4% BHO DD sample. This argument is consistent with the TEM observation discussion in figure 2.

This argument is also supported by the much improved $J_c(H)$ and $F_p(H)$ of the 6 vol% BHO DD sample at $H//ab$. As shown in figures 4(f) and (i), the $J_c(H)$ and $F_p(H)$ of this sample at 65 K are the best among the three BHO DD samples. The increasing trends of the ab -aligned APCs in both quantity and pinning efficiency with increasing BHO doping can be found in figure 5. At 65 K, the $H_{max} > 90 \text{ kOe}$ (instrument limit) for the 4% and 6% BHO DD samples is higher than $H_{max} \sim 65 \text{ kOe}$ for 2% BHO DD film at $H//ab$ -plane ($\theta = 90^\circ$). Similarly, the $F_{p,max}$ at $H//ab$ -plane is increased by 1.5 times for each additional 2% BHO concentration ($F_{p,max} \sim 31.0 \text{ GN m}^{-3}$, 54.0 GN m^{-3} and 79.0 GN m^{-3} for 2%, 4% and 6% BHO DD film respectively) as shown in figure 5(b). The twice higher $F_{p,max} \sim 79.0 \text{ GN m}^{-3}$ at $H//ab$ -plane as compared to $F_{p,max} \sim 45.78 \text{ GN m}^{-3}$ at $H//c$ -axis for the 6% BHO DD film (figure 5(b)) supports the argument of switching of 1D APCs from c -axis to ab -plane alignment by increasing tangential strain along ab -plane and compressive strain along

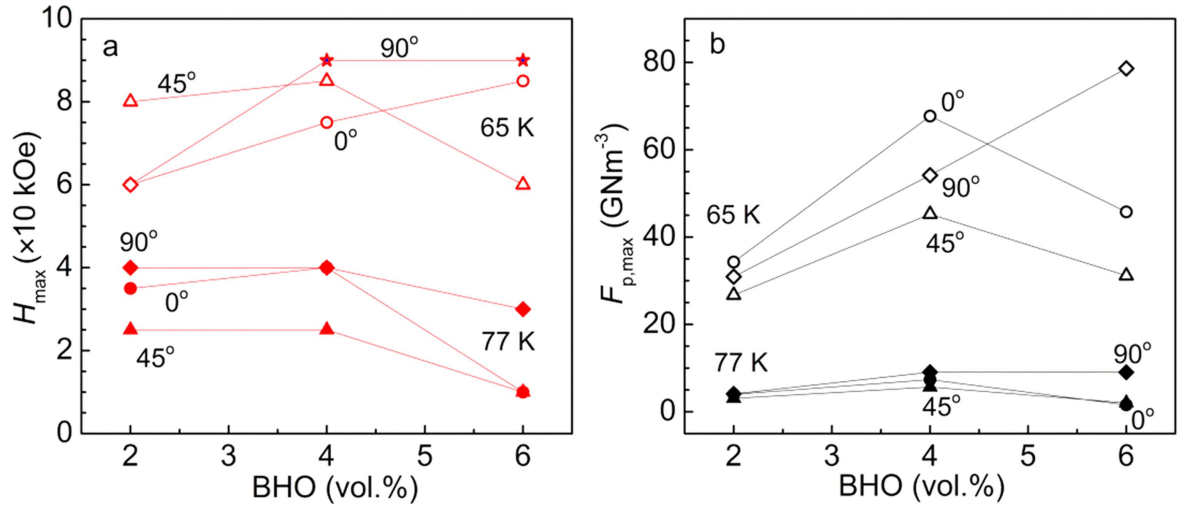


Figure 5. BHO concentration dependence of (a) H_{\max} and (b) $F_{p,\max}$ measured at 77 K (solid) and at 65 K (open), on $H//c$ -axis (circle), H at $\theta = 45^\circ$ (triangle) and $H//ab$ -plane (diamond) of 2%, 4% and 6% BHO DD nanocomposite films. ★ indicates the value from the instrument limit; this may go higher. Connecting lines are for eye catching purposes.

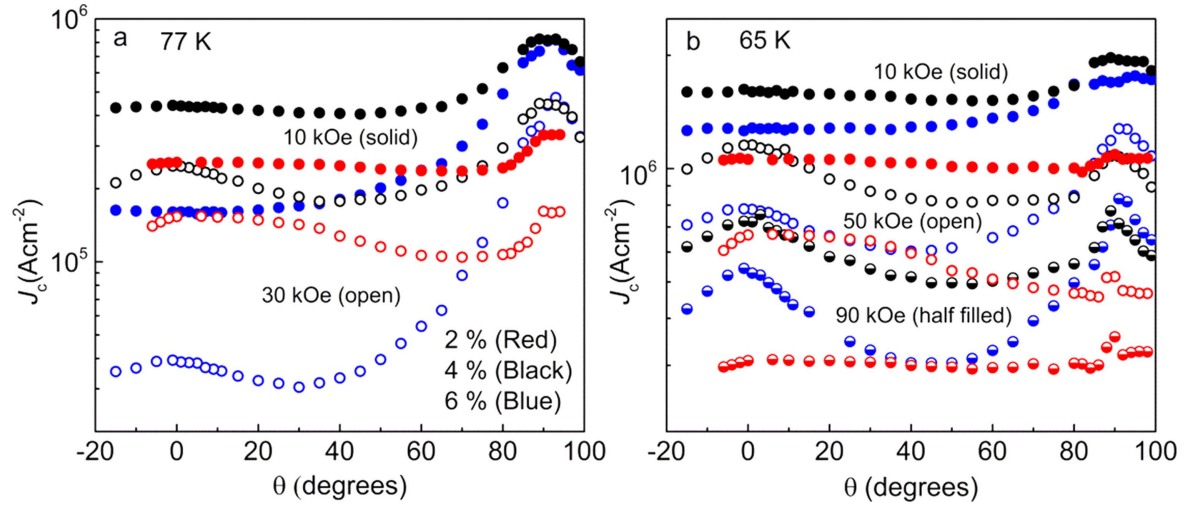


Figure 6. Angular dependence of J_c measured on 2%, 4% and 6% BHO DD nanocomposite films at (a) 77 K, and 10 kOe (solid) and 30 kOe (open), (b) 65 K, and 10 kOe (solid), 50 kOe (open), and 90 kOe (half filled) circles. Color codes follow the same for both figures.

Table 2. Alpha (α) values of 2%, 4% and 6% BHO DD films at different field orientation and temperatures.

Samples	Alpha (α) values					
	77 K			65 K		
	$H//c$	H at $\theta = 45^\circ$	$H//ab$	$H//c$	H at $\theta = 45^\circ$	$H//ab$
2.0% BHO DD	0.26	0.29	0.23	0.16	0.25	0.20
4.0% BHO DD	0.35	0.40	0.40	0.13	0.23	0.24
6.0% BHO DD	0.64	0.59	0.27	0.20	0.24	NA

c -axis (adds on by Y_2O_3 as well) with BHO concentration correlates with the APCs morphology observed in figure 2(c) for 6% BHO DD film. This trend is contrast to the similar doping of BZO (6%) in BZO DD film in which $J_c(H//c\text{-axis})$ is enhanced [20].

Figures 6(a) and (b) compare the $J_c(\theta)$ of the three BHO DD samples at the 10 and 30 kOe at 77 K, and 10, 50 and 90 kOe at 65 K, respectively. The absence of J_c valley in whole angular range from $H//c$ -axis to $H//ab$ -plane for 2 vol% BHO DD sample is an indication of strong pinning

compared to 4% and 6% BHO DD in which J_c valleys are appeared as a consequence of weaker pinning which leads to increase the J_c anisotropy. Quantitatively, the J_c anisotropy can be estimated from the ratio of $(J_{c,max} - J_{c,min})/J_{c,min}$ for the entire angular range of $\theta = 0^\circ$ ($H//c$ -axis)- 90° ($H//ab$ -plane) where $J_{c,max}$ and $J_{c,min}$ are the highest value of the peak and lowest value of the trough respectively. The J_c anisotropy $\sim 40\%$ for 2% BHO DD is less than J_c anisotropy $\sim 104\%$ for 4% BHO DD at 77 K, 10 kOe. At 65 K and 90 kOe, J_c anisotropy is reduced to $\sim 18\%$ for 2% BHO DD film is 3.0 and 9.0 times less compared to J_c anisotropy $\sim 56\%$ and 173% for 4% and 6% BHO DD film respectively indicates the strong isotropic pinning in the former compared to latter two films. The overall up lifted $J_c(\theta)$ curve with two comparable distinct peaks at $H//c$ -axis and $H//ab$ -plane at $H \sim 50$ and 90 kOe for 4 vol% BHO DD show enhanced strong pinning but not as isotropic as 2 vol% BHO DD film at the same fields. Such an overall enhancement of $J_c(\theta)$ for the entire angular range can be attributed to the mixed morphology of APCs observed in TEM images of 4% BHO DD film. At 65 K, the highest J_c anisotropy $\sim 111\%$ and 173% at 50 and 90 kOe respectively for 6% BHO DD film is due to lower $J_{c,min}$ (lack of 3D APCs) and the higher J_c peaks at $H//ab$ -plane due to strong pinning by ab -aligned 2D APCs. However, equivalent $J_{c,min}$ with comparable $J_c(\theta = 30^\circ - 60^\circ)$ for 2% and 6% BHO at 65 K and 90 kOe explores; the increased BHO concentration beyond the threshold value (4% in this study) does not improve the isotropic pinning in contrast to 6% BZO concentration in BZO DD films [20] at their optimal growth temperature. It further indicates that probably Y_2O_3 3D APCs or BHO 3D APCs are effective than misaligned BHO 1D APCs at that angular range. It is known sharp J_c peak at $H//ab$ -plane is due to intrinsic properties of YBCO but wider peak observed in 4% and 6% BHO films attribute these peaks [43]. The possible switch of 1D APCs is consistent and comparable to the switching of BZO 1D APCs from c -axis to ab -plane in the vicinal substrate as the vicinal angle increased to 15° [43]. Comparing the $J_c(\theta)$ at 77 K, 10 kOe [43], the similar trend of increasing $J_c(\theta)$ curve towards the $\theta = 90^\circ$ ($H//ab$ -plane) especially away from $\theta = 30^\circ$ attributes the distribution of BZO 1D APCs and their morphology should be similar to BHO 1D APCs in 6% BHO DD with additional Y_2O_3 3D APCs in the film.

Conclusion

In conclusion, this work has investigated the adaption of primary BHO APC morphologies to the presence of secondary Y_2O_3 APCs of 3 vol%. While a mixed 1D (in c -axis) + 2D (in ab -plane) + 3D APC landscape was present in all cases, a systematic change in the proportion of each kind of APCs was observed with an increasing BHO concentration from 2 to 6 vol%. This is primarily due to the switch of the longer (mostly through film thickness) BHO 1D APCs (in c -axis) at lower BHO concentrations to the shorter and more misaligned segments at higher BHO concentrations. Such a switch is a consequence of the adaption of BHO APCs to the

presence of 3D Y_2O_3 APCs, which are expected to impede the diffusion of BHO during film growth and to introduce local strains on APC/YBCO nanocomposites to prevent the formation of perfectly c -axis aligned BHO 1D APCs. The mixed APC morphology is beneficial for reducing J_c anisotropy in these BHO DD samples. A much smaller J_c anisotropy $\sim 18\%$ has been observed for 2% BHO DD film at high field of 90 kOe. The overall best $J_c(H, \theta)$ was observed for 4% BHO DD films at 65–77 K, suggesting DD as an effective approach for the generation of a mixed-morphology APC landscape with strong and isotropic pinning.

Acknowledgments

This research was supported in part by NSF contracts Nos: NSF-DMR-1337737 and NSF-DMR-1508494, the AFRL Aerospace Systems Directorate, and the Air Force Office of Scientific Research (AFOSR), the US National Science Foundation (DMR-1565822) for TEM characterization.

ORCID iDs

Bibek Gautam  <https://orcid.org/0000-0002-3406-8965>

Shihong Chen  <https://orcid.org/0000-0001-8762-4518>

Jijie Huang  <https://orcid.org/0000-0002-7397-1209>

References

- [1] Horide T *et al* 2016 Influence of matching field on critical current density and irreversibility temperature in $YBa_2Cu_3O_7$ films with $BaMO_3$ ($M = Zr, Sn, Hf$) nanorods *Appl. Phys. Lett.* **108** 082601
- [2] Emergo R L S *et al* 2010 The effect of thickness and substrate tilt on the BZO splay and superconducting properties of $YBa_2Cu_3O_{7-x}$ films *Supercond. Sci. Technol.* **23** 115010
- [3] Llodes A *et al* 2012 Nanoscale strain-induced pair suppression as a vortex-pinning mechanism in high-temperature superconductors *Nat. Mater.* **11** 329–36
- [4] Matsui V *et al* 2015 Current-carrying abilities of nanostructured HTS thin films *J. Nanosci. Nanoeng.* **1** 38–43
- [5] Matsumoto K and Mele P 2009 Artificial pinning center technology to enhance vortex pinning in YBCO coated conductors *Supercond. Sci. Technol.* **23** 014001
- [6] Jha A K *et al* 2014 Tuning the microstructure and vortex pinning properties of YBCO-based superconducting nanocomposite films by controlling the target rotation speed *Supercond. Sci. Technol.* **27** 25009
- [7] Mele P *et al* 2009 Systematic study of $BaSnO_3$ doped $YBa_2Cu_3O_{7-x}$ films *Physica C* **469** 1380–3
- [8] Opherden L *et al* 2016 Large pinning forces and matching effects in $YBa_2Cu_3O_{7-\delta}$ thin films with Ba_2Y (Nb/Ta) O_6 nano-precipitates *Sci. Rep.* **6** 21188
- [9] Wee S *et al* 2013 Self-assembly of nanostructured, complex, multication films via spontaneous phase separation and strain-driven ordering *Adv. Funct. Mater.* **23** 1912–8
- [10] Miura S *et al* 2015 Vortex pinning at low temperature under high magnetic field in $SrBa_2Cu_3O_y$ superconducting films with high number density and small size of $BaHfO_3$ nanorods *Supercond. Sci. Technol.* **28** 114006

- [11] Erbe M *et al* 2015 BaHfO₃ artificial pinning centres in TFA-MOD-derived YBCO and GdBCO thin films *Supercond. Sci. Technol.* **28** 114002
- [12] Tran D H *et al* 2014 A close correlation between nanostructure formations and the thickness dependence of the critical current density in pure and BaSnO₃ added GdBa₂Cu₃O_{7-x} films *J. Appl. Phys.* **115** 163901
- [13] Tobita H *et al* 2012 Fabrication of BaHfO₃ doped Gd₁Ba₂Cu₃O_{7-δ} coated conductors with the high I_c of 85 A/cm-w under 3 T at liquid nitrogen temperature (77 K) *Supercond. Sci. Technol.* **25** 062002
- [14] Miura S *et al* 2016 Flux pinning properties in BaHfO₃-Doped SmBa₂Cu₃O_y films on metallic substrates fabricated with low temperature growth *IEEE Trans. Appl. Supercond.* **26** 1–5
- [15] Senatore C *et al* 2015 Field and temperature scaling of the critical current density in commercial REBCO coated conductors *Supercond. Sci. Technol.* **29** 014002
- [16] Selvamanickam V *et al* 2015 High critical currents in heavily doped (Gd, Y)Ba₂Cu₃O_x superconductor tapes *Appl. Phys. Lett.* **106** 032601
- [17] Horide T *et al* 2013 J_c improvement by double artificial pinning centers of BaSnO₃ nanorods and Y₂O₃ nanoparticles in YBa₂Cu₃O₇ coated conductors *Supercond. Sci. Technol.* **26** 075019
- [18] Awaji S *et al* 2011 Anisotropy of the critical current density and intrinsic pinning behaviors of YBa₂Cu₃O_y coated conductors *Appl. Phys. Express* **4** 13101
- [19] Sebastian M A P *et al* 2017 Study of the flux pinning landscape of YBCO thin films with single and mixed phase additions BaMO₃ + Z: M = Hf, Sn, Zr and Z = Y₂O₃, Y₂₁₁ *IEEE Trans. Appl. Supercond.* **27** 1–5
- [20] Chen S *et al* 2017 Enhancement of isotropic pinning force in YBCO films with BaZrO₃ nanorods and Y₂O₃ nanoparticles *IEEE Trans. Appl. Supercond.* **27** 1–5
- [21] Wu J *et al* 2015 Controlling BaZrO₃ nanostructure orientation in YBa₂Cu₃O₇ films for a three-dimensional pinning landscape *Supercond. Sci. Technol.* **28** 125009
- [22] Jha A K *et al* 2015 Tailoring the vortex pinning strength of YBCO thin films by systematic incorporation of hybrid artificial pinning centers *Supercond. Sci. Technol.* **28** 114004
- [23] Baca F *et al* 2009 Control of BaZrO₃ nanorod alignment in YBa₂Cu₃O_{7-x} thin films by microstructural modulation *Appl. Phys. Lett.* **94** 102512
- [24] Sebastian M A P *et al* 2013 Optimizing flux pinning of YBCO superconductor with BaSnO₃ + Y₂O₃ dual mixed phase additions *IEEE Trans. Appl. Supercond.* **23** 8002104
- [25] Maiorov B *et al* 2009 Synergetic combination of different types of defect to optimize pinning landscape using BaZrO₃ doped YBa₂Cu₃O₇ *Nat. Mater.* **8** 398–404
- [26] Baca J F *et al* 2013 Interactive growth effects of rare-earth nanoparticles on nanorod formation in YBa₂Cu₃O_x thin films *Adv. Funct. Mater.* **23** 4757–869
- [27] Jha A K *et al* 2015 Systematic variation of hybrid APCs into YBCO thin films for improving the vortex pinning properties *IEEE Trans. Appl. Supercond.* **25** 1–5
- [28] Selvamanickam V *et al* 2015 Critical current density above 15 MA cm⁻² at 30 K, 3 T in 2.2 μm thick heavily-doped (Gd, Y)Ba₂Cu₃O_x superconductor tapes *Supercond. Sci. Technol.* **28** 072002
- [29] Obradors X and Puig T 2014 Coated conductors for power applications: materials challenges *Supercond. Sci. Technol.* **27** 044003
- [30] Mele P *et al* 2014 High pinning performance of YBa₂Cu₃O_{7-x} films added with Y₂O₃ nanoparticulate defects *Supercond. Sci. Technol.* **28** 024002
- [31] Wu J and Shi J 2017 Interactive modeling-synthesis-characterization approach towards controllable *in situ* self-assembly of artificial pinning centers in RE-123 films *Supercond. Sci. Technol.* **30** 103002
- [32] Shi J J and Wu J Z 2012 Micromechanical model for self-organized secondary phase oxide nanorod arrays in epitaxial YBa₂Cu₃O_{7-δ} films *Phil. Mag.* **92** 2911–22
- [33] Shi J J and Wu J Z 2012 Structural transition of secondary phase oxide nanorods in epitaxial YBa₂Cu₃O_{7-δ} films on vicinal substrates *Phil. Mag.* **92** 4205–14
- [34] Gautam B *et al* 2017 Transformational dynamics of BZO and BHO nanorods imposed by Y₂O₃ nanoparticles for improved isotropic pinning in YBa₂Cu₃O_{7-δ} thin films *AIP Adv.* **7** 075308
- [35] Sieger M *et al* 2015 BaHfO₃-doped thick YBa₂Cu₃O_{7-δ} films on highly alloyed textured Ni–W tapes *IEEE Trans. Appl. Supercond.* **25** 1–4
- [36] Mele P *et al* 2008 Ultra-high flux pinning properties of BaMO₃-doped YBa₂Cu₃O_{7-x} thin films (M = Zr, Sn) *Supercond. Sci. Technol.* **21** 032002
- [37] Wu J Z *et al* 2014 The effect of lattice strain on the diameter of BaZrO₃ nanorods in epitaxial YBa₂Cu₃O_{7-δ} films *Supercond. Sci. Technol.* **27** 044010
- [38] Guzman R *et al* 2013 Strain-driven broken twin boundary coherence in YBa₂Cu₃O_{7-x} nanocomposite thin films *Appl. Phys. Lett.* **102** 81906
- [39] Cantoni C *et al* 2011 Strain-driven oxygen deficiency in self-assembled, nanostructured, composite oxide films *ACS Nano* **5** 4783–9
- [40] Watanebe M *et al* 2014 Experimental study in the development of HTS NMR probe *J. Phys.: Conf. Ser.* **507** 012051
- [41] Jha A K, Khare N and Pinto R 2012 Comparison of flux pinning mechanism in laser ablated YBCO and YBCO: BaZrO₃ nanocomposite thin films *J. Supercond. Novel Magn.* **25** 377–80
- [42] Klaassen F *et al* 2001 Vortex pinning by natural linear defects in thin films of YBa₂Cu₃O_{7-δ} *Phys. Rev. B* **64** 184523
- [43] Wu J *et al* 2015 Probing microscopic strain interplay due to impurity doping and vicinal growth and its effect on pinning landscape in YBCO films *IEEE Trans. Appl. Supercond.* **25** 1–5